LIMNOLOGY AND OCEANOGRAPHY
Letters

ASLO
Open Access

Limnology and Oceanography Letters 9, 2024, 634–643

doi: 10.1002/lol2.10416

LETTER

Energy inputs imprint seasonality and fractal structure on river metabolic regimes

Yuseung Shin[1]*, *James W. Jawitz*[2], *Matthew J. Cohen*[3]

[1]School of Natural Resources and Environment, University of Florida, Gainesville, Florida, USA; [2]Soil, Water, and Ecosystem Sciences Department, University of Florida, Gainesville, Florida, USA; [3]School of Forest, Fisheries, and Geomatics Sciences, University of Florida, Gainesville, Florida, USA

Scientific Significance Statement

Temporal variation of primary production and respiration in rivers (i.e., river metabolism) is a complex response to temperature, energy inputs (light, organic carbon), nutrient supply, flow, and stream network position. Despite recent proliferation of long-term high-resolution data on river metabolism, generalizations about the structure and controls of temporal variation remain limited. Here we asked: what are the dominant temporal patterns of river metabolism, and how are these patterns affected by environmental factors? Our approach to answering these questions partitions metabolism time series into signals of different frequencies, ranging from days to years, revealing a dominant mode of seasonal variation and self-similar, or fractal, patterns across all other time scales. Our results strongly implicate the role of energy availability on controlling variation in river metabolism.

Abstract

The temporal structures of gross primary production (GPP) and ecosystem respiration (ER) vary across time scales in response to complex interactions among dynamic drivers (e.g., flow, light, temperature, organic matter supply). To explore emergent patterns of river metabolic variation, we applied frequency-domain analysis to multiyear records of metabolism across 87 US rivers. We observed a dominant annual periodicity in metabolic variation and universal fractal scaling (i.e., power spectral density inversely correlated with frequency) at sub-annual frequencies, suggesting these are foundational temporal structures of river metabolic regimes. Frequency-domain patterns of river metabolism aligned best with drivers related to energy inputs: benthic light for GPP and GPP for ER. Simple river metabolism models captured frequency-domain patterns when parameterized with appropriate energy inputs but neglecting temperature controls. These results imply that temporal

*Correspondence: yuseungshin@ufl.edu

Associate editor: James B. Heffernan

Author Contribution Statement: All authors conceived the research questions. YS and MJC designed the study. YS collected the data, conducted the analysis, and wrote the paper. All authors contributed to the interpretation and revision of the drafts.

Data Availability Statement: Data and R codes used in this study are available in a CUAHSI Hydroshare repository (https://doi.org/10.4211/hs.6663122ba06749ac92409ff53f81af7c).

Additional Supporting Information may be found in the online version of this article.

variation of energy supply imprints directly on metabolic signals and that frequency-domain patterns provide benchmark properties to predict river metabolic regimes.

The metabolic regime concept describes the temporal structure of variation in gross primary production (GPP) and ecosystem respiration (ER) in flowing waters (Bernhardt et al. 2018). Metabolic regimes arise from interactions among biotic and abiotic drivers (e.g., organic matter [OM] loading, light, flow, temperature), exploration of which has only recently been possible from advances in dissolved oxygen (DO) sensors and models translating DO signals into metabolic fluxes (Appling et al. 2018*a*). Emergence of multiannual river metabolism data (Appling et al. 2018*b*) has yielded insights about productivity archetypes (Savoy et al. 2019), state transitions (Diamond et al. 2022), emergent network behaviors (Koenig et al. 2019), and the foundational importance of light and flow for predicting annual metabolic fluxes (Bernhardt et al. 2022). While these synthesis datasets have largely informed time-series statistics (e.g., timing and magnitude of seasonality, annual mean), they can also inform the embedded temporal structure of metabolism and discern drivers of this variation across time scales.

River metabolism describes solar energy capture by autotrophs and stored energy use by heterotrophs (Odum 1956), suggesting temporal patterns of energy flows control metabolic variation. Network position and flow control light inputs and OM loading, yielding archetypal spatiotemporal patterns of metabolism (Vannote et al. 1980). Because insolation is influenced by canopy and water-column attenuation (Kirk et al. 2021; Savoy and Harvey 2021), benthic light describes energy available to river autotrophs (Julian et al. 2011). Similarly, flow affects OM availability (Uehlinger 2006; Demars 2019), controlling temporal dynamics of energy availability for respiration. A focus on energy controls recently prompted development of river metabolism models containing latent biomass effects to predict GPP (Blaszczak et al. 2023) and multiple OM sources (flow, GPP, litter) to predict ER (Bertuzzo et al. 2022). Despite these advances, model skill for predicting metabolic regime structure (i.e., variation at different time scales) remains untested.

Time series can be converted into the frequency domain by partitioning temporal variance into signals at different frequencies, known as power spectra (Stoica and Moses 2005). This retains overall variation, and reveals frequencies at which variation is large and, by extension, alignment with time-varying drivers (Cazelles et al. 2007). One common pattern for environmental time series is fractal scaling, where variance is equal (i.e., self-similar) at all time scales, revealed as an inverse association between frequency and signal strength at that frequency (Halley 1996). In catchment export signals, frequency-domain analysis reveals fractal scaling of solute chemistry (Kirchner and Neal 2013) and landscape filtering between rainfall and streamflow signals (Molénat et al. 1999), strongly implicating catchment storage in signal genesis. Channel storage imprints multifractal signals (i.e., power spectra exhibiting distinct scaling exponents) with variance dampening at time scales shorter than network residence times (Hensley et al. 2018). Frequency-domain analysis revealed variance alignment of terrestrial metabolism with climate drivers across time scales (Stoy et al. 2009), but this approach has not been applied to riverine metabolism.

Here, we use spectral analysis to evaluate temporal structures of river metabolism, focusing on evidence for dominant periodicities and signal alignment with hypothesized controls (OM loading, light, temperature, discharge). We used multiyear data across the United States to test two hypotheses: (1) metabolic variance is best aligned with energy availability dynamics, specifically benthic light for productivity and organic inputs, including GPP, for respiration, and (2) incorporating key drivers into metabolism models improves predictions of observed frequency-domain patterns. By generalizing frequency-domain patterns of river metabolism, we provide a novel tool to describe metabolic regimes and assess model predictions.

Methods

Data

Daily metabolism data, with hourly discharge (Q) and water temperature (T), were from Appling et al. (2018*b*), a dataset containing 356 multiyear records of GPP and ER modeled from diurnal DO variation (Odum 1956) using *streamMetabolizer* (Appling et al. 2018*a*). Sites reporting less than 2 yr of data or > 25% missing data were excluded. Unrealistic values (negative GPP, positive ER) were omitted. We used hourly estimates of surface and benthic irradiance (PAR_S, PAR_B) from Savoy and Harvey (2021), who modified open-sky irradiance (PAR_O) considering canopy and water-column (i.e., depth, turbidity) attenuation. Requisite overlap between metabolism and irradiance datasets yielded 87 sites (50 for GPP, 74 for ER) (Shin 2024; Supporting Information Table S1).

Spectral analysis

Time series were translated into the frequency domain (Fig. 1a,b) with the *spectrum* function in R (Core Team 2013), yielding periodic oscillation strength (i.e., power spectral density; PSD) at each frequency (Stoica and Moses 2005). Data processing for spectral analysis (interpolation, aliasing) is explained in the Supporting Information (Text S1). We focused on intra-annual frequencies (i.e., $>1/365$ d^{-1}); as datasets mature, inter-annual frequencies will become tractable. Names of extracted variables and their meaning are summarized in Table 1.

Seasonality manifests at annual frequency in the PSD (PSD_A). To standardize seasonal signal strength across sites

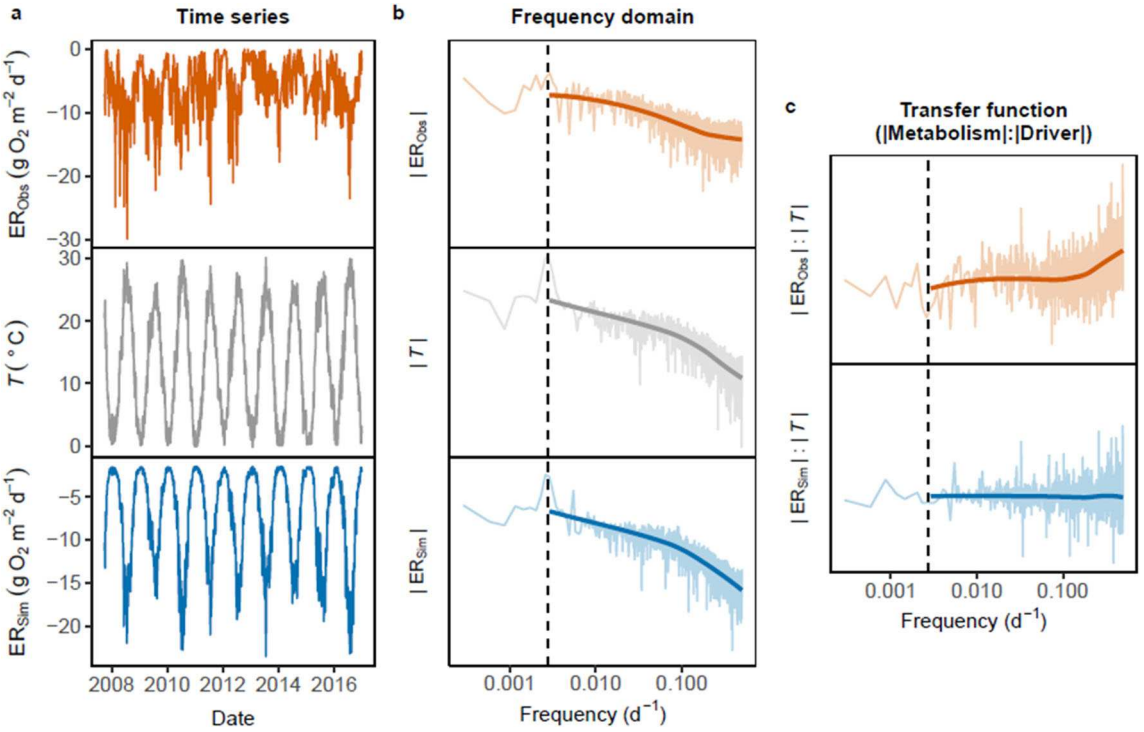

Fig. 1. (**a**) Time series for the Delaware River at Trenton, New Jersey, of observed ER (ER_{Obs}), T, and simulated ER (ER_{Sim}) based on T using the Arrhenius equation (Eq. 5), which sequentially converted to (**b**) frequency domains and (**c**) transfer functions between ER and T. Annual frequency is marked by vertical dashed lines at 1/365 d^{-1}. Thick lines are from locally estimated scatterplot smoothing (LOESS). A transfer function slope near zero, as in the bottom graph of (**c**), indicates variability in T is directly imprinted on ER_{Sim}, while the rising transfer function slope at high frequency in the upper graph of (**c**) indicates that T and ER_{Obs} become decoupled at these frequencies and some other less persistent driver controls fine-scale ER variation.

Table 1. Summary of key variables and abbreviations.

Abbreviation	Definition	Significance
PSD	Power spectral density	Strength of periodic oscillation
RSS	Relative strength of seasonality (log-scale PSD ratio of annual to intra-annual frequencies)	Standardized seasonal signal strength with divergent total variance
α	Spectral slope	Signal persistence
	(log-scale slope between PSD and frequency)	$\alpha = 0$: random variation (white noise)
		$\alpha = 1$: self-similar variation (fractal or pink noise)
		$\alpha = 2$: random-walk variation (Brown noise)
α_{Inter}	α at intermediate frequencies	Persistence at 0.01–0.1 d^{-1} (10–100 d)
α_{High}	α at high frequencies	Persistence at > 0.1 d^{-1} (< 10 d)
TF	Transfer function	Alteration of temporal variation from input (a driver) to output (metabolism) functions
α_{TF}	Spectral slope of TF	Variation alteration from input to output
		$\alpha_{TF} = 0$: Variation aligned (imprinted)
		$\alpha_{TF} > 0$: Variation damped
		$\alpha_{TF} < 0$: Variation amplified
$\alpha_{TF,Inter}$	α_{TF} at intermediate frequencies	Variation alteration at 0.01–0.1 d^{-1} (10–100 d)
$\alpha_{TF,High}$	α_{TF} at high frequencies	Variation alteration at > 0.1 d^{-1} (< 10 d)

with divergent total variance, we quantified the relative strength of seasonality (RSS) comparing PSD_A to mean intra-annual PSD ($\overline{PSD_I}$):

$$RSS = \log\left(\frac{PSD_A}{\overline{PSD_I}}\right) \quad (1)$$

Inverse PSD variation with frequency (f) implies systematic variance damping at higher frequencies (Kirchner and Neal 2013):

$$PSD \propto \frac{1}{f^{\alpha}} \quad (2)$$

where spectral slope, α, quantifies signal persistence, or the memory of previous time steps. A flat slope ($\alpha = 0$; white noise) indicates no persistence (i.e., stochastic random variation), while a steep slope ($\alpha = 2$; Brown noise) describes strong persistence (i.e., random-walk variation). Between these extremes is fractal scaling ($\alpha = 1$; $1/f$ or pink noise) which is both stochastic and persistent with equal importance of all constituent time scales (i.e., self-similar variation).

We obtained α from linear regression of log-transformed PSD and frequency. Power spectra were smoothed to reduce signal noise using logarithmic binning (Thompson and Katul 2012). Multiple PSD peaks at $f < \sim 0.01\,d^{-1}$ (100 d) and a clear slope break in PSD at $f \approx 0.1\,d^{-1}$ (10 d) for most abiotic factors, especially T, necessitated separate α estimates at intermediate (0.01–0.1 d^{-1}; α_{Inter}) and high (>0.1 d^{-1}; α_{High}) frequencies. Low-frequency PSD (<0.01 d^{-1}) were confounded by effects of annual periodicity, precluding slope estimation.

Transfer function

The convolution of two time series is expressed as their product in frequency domain such that coupling between metabolism and drivers is expressed as:

$$|M| = |D| \times |H| \quad (3)$$

where $|M|$, $|D|$, and $|H|$ are absolute values of PSDs of metabolism, a driver, and a transfer function (TF) defined as PSD ratio between metabolism and a driver (i.e., $|H| = |M| / |D|$). Transfer functions indicate how input temporal structures are altered in the output, revealing alignment or divergence across frequencies (Stoy et al. 2009).

We assessed TFs for each driver independently, quantifying the transfer function slope (α_{TF}) for GPP in response to T, Q, PAR_S, and PAR_B, and for ER in response to T, Q, and GPP. Alignment of metabolism and driver spectra (i.e., $\alpha_{TF} = 0$; Fig. 1c, bottom) implies direct transfer of variance structure from driver to metabolism, or minimal filtering (Molénat et al. 1999). In contrast, $\alpha_{TF} \neq 0$ implies filtering effects that damp ($\alpha_{TF} > 0$) the signal by storage or response lags (e.g., hillslope and channel storage effects on solute variation; Hensley et al. 2018) or amplify ($\alpha_{TF} < 0$) by decoupling of variance structures (Fig. 1c, top). We calculated α_{TF} using separate linear regressions on log-transformed TFs for intermediate ($\alpha_{TF,Inter}$) and high frequencies ($\alpha_{TF,High}$), informing coupling at different time scales. The 95% confidence interval of fitted α_{TF} values quantified departure from zero.

Metabolism simulation

To assess how metabolism models align with observed variance structures, we simulated GPP and ER with different drivers. We compared irradiance inputs (PAR_O, PAR_S, PAR_B) on GPP predictions using a photosynthesis saturation model (Jassby and Platt 1976) with an activation energy function (Brown et al. 2004):

$$GPP = P_{max} \tanh\left(\frac{A_P I}{P_{max}}\right) e^{-\frac{E_{a,GPP}}{k_B}\left(\frac{1}{T}-\frac{1}{T_C}\right)} \quad (4)$$

where P_{max} $\left(g\,O_2\,m^{-2}\,h^{-1}\right)$ is maximum GPP at reference temperature T_C (K), A_P $\left(g\,O_2\,s\,\mu mol^{-1}\,photon\,h^{-1}\right)$ is the GPP vs. irradiance I $\left(\mu mol\,photon\,m^{-2}\,s^{-1}\right)$ slope, $E_{a,GPP}$ (eV) is GPP activation energy, k_B is the Boltzmann constant $\left(eV\,K^{-1}\right)$, and T (K) is water temperature (Supporting Information Table S2 contains values). Although A_P and $E_{a,GPP}$ vary across sites, we initially used $A_P = 0.001P_{max}$ reflecting low likelihood of light saturation (Dodds et al. 1999), and constrained $E_{a,GPP}$ to theoretical values (0.32 eV, Allen et al. 2005). We also examined the models with A_p and $E_{a,GPP}$ varied over ranges $0.001P_{max}$ to $0.01P_{max}$ in $0.0001P_{max}$ steps and 0–1.2 eV in 0.01 eV steps. The latter range precluded implausibly large values (e.g., up to ~8.7 eV; Song et al. 2018). Simulated hourly GPP was summed to yield daily rates.

While ER models often solely depend on T (Parkhill and Gulliver 1999), we compared three ER model configurations with and without OM supplies (T, $T + Q$, $T + Q +$ GPP).

$$ER_T = R_C\, e^{-\frac{E_{a,ER}}{k_B}\left(\frac{1}{T}-\frac{1}{T_C}\right)} \quad (5)$$

where R_C $\left(g-O_2\,m^{-2}\,d^{-1}\right)$ is respiration at T_C and $E_{a,ER}$ (eV) is ER activation energy (Supporting Information Table S2), which is theoretically 0.65 eV (Allen et al. 2005). We also varied $E_{a,ER}$ over the same range as $E_{a,GPP}$. We added dissolved organic carbon (DOC) supply as a function of Q to Eq. 5 based on Fasching et al. (2016):

$$ER_{T,Q} = \left(\frac{\delta_Q + Q^{\gamma_Q}}{\delta_Q + Q_{max}^{\gamma_Q}}\right) R_C\, e^{-\frac{E_{a,ER}}{k_B}\left(\frac{1}{T}-\frac{1}{T_C}\right)} \quad (6)$$

where Q $\left(L\,s^{-1}\right)$ and Q_{max} are site daily mean and site maximum discharge. We used an empirical power-function

([DOC] = $\delta_Q + Q^{\gamma_Q}$ with $\delta_Q = 4.7$ and $\gamma_Q = 0.4$; Segatto et al. 2020) for DOC concentrations, implying maximum respiration at Q_{max}. Lastly, we included GPP using a simplified ER model with varying C sources (Bertuzzo et al. 2022):

$$\mathrm{ER}_{T,Q,\mathrm{GPP}} = \left(\frac{\delta_Q + Q^{\gamma_Q}}{\delta_Q + Q_{\max}^{\gamma_Q}} + \frac{\mathrm{GPP}}{\mathrm{GPP}_{\max}}\right) R_C \, e^{-\frac{E_{a,ER}}{k_B}\left(\frac{1}{T} - \frac{1}{T_C}\right)} \quad (7)$$

which assumes maximum respiration at the site maximum GPP (GPP_{max}).

Frequency-domain model performance was assessed using divergence of PSD features (RSS, α_{Inter}, α_{High}) between observations and simulations (Obs − Sim). To compare model performance across E_a and A_P values, we used cross-site mean divergence ([Obs − Sim]). We obtained time-domain goodness-of-fit (normalized root-mean-square error [NRMSE] = [RMSE/observed interquartile range] and R^2) for each site using nonlinear least-squares regression for parameter estimation (P_{max}, R_C, A_P, $E_{a,GPP}$, $E_{a,ER}$). Model comparison in both frequency and time domains informs whether models can explain the timing of variation and the temporal structures of metabolic regimes.

We further analyzed metabolism predictions from two alternative models to assess their frequency-domain alignment with observations. Blaszczak et al. (2023) used autoregressive (AR) and latent biomass (LB) models to predict GPP. Bertuzzo et al. (2022) used multiple C sources to predict ER. We assessed these models in time and frequency domains.

Results

Frequency-domain patterns

Across sites, we observed a metabolism annual PSD peak (Fig. 2a,b) orders of magnitude greater than intra-annual mean PSD ($\mathrm{RSS}_{GPP} = 2.52 \pm 0.34$, $\mathrm{RSS}_{ER} = 2.34 \pm 0.53$). The RSS of both PAR_S and PAR_B strongly correlated with RSS_{GPP} ($r = 0.48$ and 0.51, respectively), but PAR_B ($\mathrm{RSS}_{PARB} = 2.29 \pm 0.63$) matched GPP better than PAR_S ($\mathrm{RSS}_{PARS} = 2.90 \pm 0.54$). RSS_{ER} was strongly coupled with RSS_{GPP} ($r = 0.65$). T and Q ($\mathrm{RSS}_T = 3.77 \pm 0.22$, $\mathrm{RSS}_Q = 1.76 \pm 0.64$) were more and less seasonal than metabolism, respectively.

Power spectra of both GPP and ER exhibited $\sim 1/f$ scaling at intra-annual frequencies (α_{Inter} and $\alpha_{High} \approx 1$) (Fig. 2c,d; Supporting Information Table S3). In contrast, most drivers deviated substantially from $1/f$ scaling at high frequency

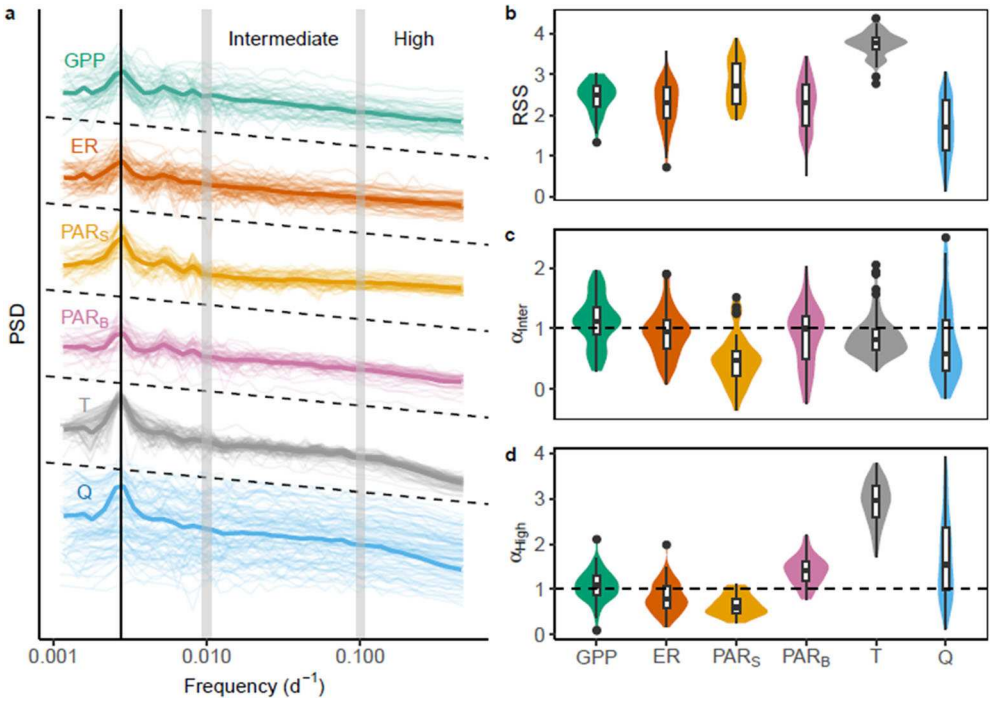

Fig. 2. (**a**) Power spectral densities (PSDs) for GPP, ER, surface and benthic PAR, *T*, and *Q* ($n = 50$ for GPP and PAR, $n = 74$ for ER, and $n = 87$ for *T* and *Q*), with each site presented as a thin line, and the mean across sites indicated by thicker lines. Vertical solid line indicates annual frequency (1/365 d^{-1}). Vertical gray bars at 0.01 and 0.1 d^{-1} (100 and 10 d in time domain) separate intermediate and high-frequency ranges at which spectral slopes for abiotic drivers clearly depart from $1/f$ scaling (dashed lines). Boxplots of (**b**) relative strength of seasonality (RSS; log scaled ratio between PSD_A vs. $\overline{\mathrm{PSD}_I}$), and (**c**) spectral slopes in intermediate (α_{Inter}) and (**d**) high-frequency ranges (α_{High}). Spectral slope $\alpha = 1$ for $1/f$ scaling is shown as a horizontal dashed line in (**c**) and (**d**). These results show universally strong seasonality in total variance and $\sim 1/f$ scaling of GPP and ER, whose spectral attributes are different from abiotic drivers.

($\alpha_{High} \geq 1$), especially for T, suggesting greater persistence than GPP or ER. PAR_S, however, showed low persistence across intra-annual time scales (α_{Inter} and $\alpha_{High} < 1$). Universal patterns of seasonality and $\sim 1/f$ scaling suggests core features of metabolic regimes, with surprisingly consistent spectral attributes of metabolism (narrow distributions) across sites (Fig. 2b–d).

Transfer functions help discriminate among drivers by assessing variance alignment across frequencies (Fig. 3; Supporting Information Table S4). At intermediate frequencies, GPP was strongly aligned with T and PAR_B ($\alpha_{TF,Inter} = 0.22 \pm 0.53$ and 0.25 ± 0.53), with most sites exhibiting $\alpha_{TF,Inter} \approx 0$, while alignments with PAR_S and Q were worse ($\alpha_{TF,Inter} = 0.65 \pm 0.62$ and 0.45 ± 0.67). At high frequency, light inputs (PAR_S, PAR_B; $\alpha_{TF,High} = 0.40 \pm 0.42$ and -0.36 ± 0.35) aligned best with GPP variance, with $\alpha_{TF,High} \approx 0$ at half the sites, and worse with T or Q ($\alpha_{TF,High} = -1.85 \pm 0.40$ and -0.46 ± 1.00). Opposite signs of $\alpha_{TF,High}$ for PAR_S and PAR_B implies high-frequency GPP variance is less dynamic than PAR_S but more dynamic than PAR_B. Variability of $\alpha_{TF,High}$ between GPP and Q was large, with just 30% of sites exhibiting $\alpha_{TF,High} \approx 0$. We note a dramatic contrast between GPP and T at high frequency ($\alpha_{TF,High} \ll 0$).

ER was best aligned with GPP across frequencies, though mean α_{TF} between ER and GPP was slightly negative, suggesting weak signal dampening ($\alpha_{TF,Inter} = -0.21 \pm 0.42$, $\alpha_{TF,High} = -0.25 \pm 0.38$; Fig. 3; Supporting Information Table S4). ER was aligned with T and Q at intermediate frequency ($\alpha_{TF,Inter} = 0.09 \pm 0.45$ and 0.22 ± 0.54) but divergent at high frequency ($\alpha_{TF,High} = -2.14 \pm 0.54$ and -0.82 ± 0.83).

While TFs helped discriminate among drivers of GPP and ER, temporal correlation analysis did not (Supporting Information Fig. S4). All drivers were weakly correlated with observed metabolism (cross-site mean correlation < 0.5), implying time-domain patterns of metabolism are poorly constrained.

Frequency-domain model assessment

Simple metabolism simulations (Eqs. 4–7) performed poorly in the time domain (mean $R^2 < 0.3$), precluding differentiation among key drivers (Supporting Information Figs. S5, S6). Across sites, time-domain goodness-of-fit (NRMSE, R^2) for the GPP model (Eq. 4) varied minimally among irradiance inputs. The models in Blaszczak et al. (2023) performed better but were variable ($0.0 < R^2 < 0.6$, mean $R^2 = 0.36$; Supporting Information Table S5), though the datasets do not overlap. For ER, our simple models (Eqs. 5–7) were less accurate than the model in Bertuzzo et al. (2022) (Supporting Information Table S6).

In contrast, frequency-domain attributes (RSS, α_{Inter}, α_{High}) clearly differentiated among drivers. For GPP, the best match (Obs – Sim ≈ 0) was using PAR_B for irradiance (Eq. 4), whereas using PAR_O and PAR_S overestimated seasonality (RSS) and underestimated intra-annual persistence (Fig. 4a). While RSS alignment varied over $E_{a,GPP}$ values, RSS was best simulated ([Obs – Sim] ≈ 0) with PAR_B and the expected $E_{a,GPP} \approx 0.32$ eV (Fig. 5, top row). Simulated spectral slopes (α_{Inter}, α_{High}) were insensitive to $E_{a,GPP}$ using PAR_B, implying a negligible role of T on GPP variance given PAR_B. Spectral slopes were more sensitive to $E_{a,GPP}$ using PAR_O and PAR_S but these outperformed PAR_B only at anomalously high $E_{a,GPP}$ (~ 0.6 and ~ 0.9 eV, respectively). GPP simulations were similarly insensitive to A_P using PAR_B but sensitive using PAR_O and PAR_S (Supporting Information Fig. S7).

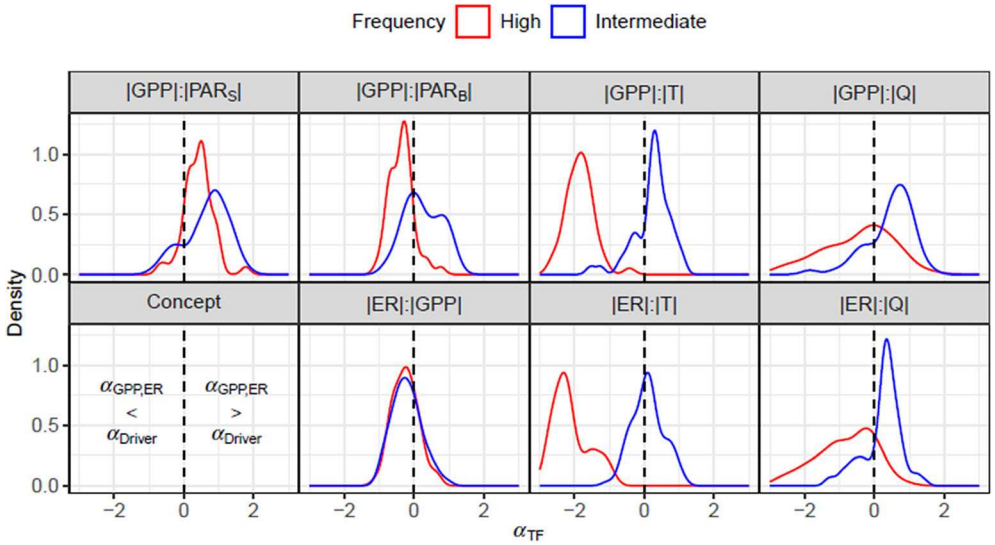

Fig. 3. Spectral slopes of transfer functions (α_{TF}) at intermediate and high-frequency ranges ($n = 50$ for GPP and $n = 74$ for ER). Vertical dashed line indicates $\alpha_{TF} = 0$, where the metabolic variance aligns perfectly with that of a driver. The result suggests different time-scale effect of each driver on GPP and ER.

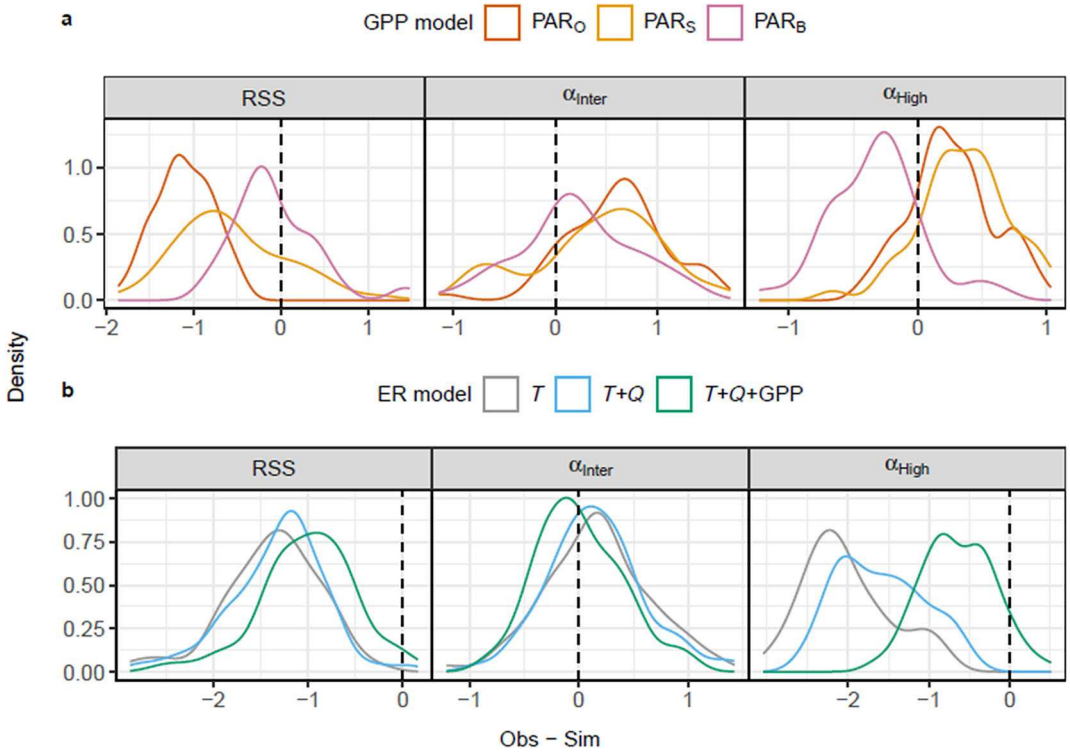

Fig. 4. Model performances for (**a**) GPP and (**b**) ER evaluated by difference between the observation and simulation (Obs − Sim) of relative strength of seasonality (RSS; left) and spectral slope at intermediate (α_{Inter}; middle) and high (α_{High}; right) frequency ranges. Difference of 0 between observation and simulation (Obs − Sim = 0; vertical dashed line) indicates perfect prediction. While GPP model (Eq. 4) using PAR$_B$ showed impressive prediction, all ER models (Eqs. 5–7) over-imposed seasonality strength and high-frequency persistence.

All ER models (Eqs. 5–7) overestimated (i.e., Obs − Sim $\ll$ 0) seasonality and high-frequency persistence (α_{High}) (Fig. 4(B)). However, neglective temperature sensitivity ($E_{a,ER} \approx 0$) improved RSS and α_{High} simulations when including Q and GPP (Fig. 5, bottom row). Even at intermediate frequency, where all models reasonably predicted α_{Inter}, the effect of $E_{a,ER}$ variation was not significant, underscoring minimal impacts of T and core importance of C sources for ER regimes.

Models considering complementary pathways and biomass memory yielded comparable frequency-domain model fit with simpler models (Eqs. 4–7). For GPP, the LB model of Blaszczak et al. (2023) captured frequency-domain patterns as well as our GPP model (Eq. 4) using PAR$_B$, outperforming their AR model, which severely overestimated persistence across frequencies (Fig. 5, top row). Frequency-domain performance of the more complex ER model of Bertuzzo et al. (2022) matched our simpler $T + Q +$ GPP model (Eq. 7) with minimal temperature sensitivity ($E_{a,ER} \approx 0$) (Fig. 5, bottom row).

Discussion

Dominant seasonality and fractal scaling

Seasonality (i.e., annual periodicity) is clearly revealed by frequency-domain analysis as the dominant structure of river metabolic regimes. While seasonality can be obscured in time series by canopy and water-column light attenuation effects on GPP (Savoy et al. 2019) and episodic allochthonous input effects on fine-scale variation of ER (Roberts et al. 2007), these intra-annual interactions yield no clear periodicity other than annual (Fig. 2).

At sub-annual time scales, we observed universal $\sim 1/f$ (i.e., fractal) scaling of metabolic temporal variation (Fig. 2). Spectral slopes were steeper than white noise (i.e., $\alpha \sim 0$) but shallower than random-walk variation (i.e., $\alpha \sim 2$) (Halley 1996; Vasseur and Yodzis 2004). Consistent persistence (i.e., $\alpha \sim 1$) across frequencies implies memory effects on metabolic variation at intra-annual time scales, possibly indicating metabolic resilience arising from biomass effects (Blaszczak et al. 2023).

Drivers of metabolic regimes

Benthic light (PAR$_B$) was the primary driver of GPP variance patterns, aligning with all spectral properties (RSS, α_{Inter}, α_{High}) of GPP (Figs. 2, 3), consistent with PAR$_B$ performance predicting GPP (Kirk et al. 2021; Savoy and Harvey 2021). However, at high frequency, α_{TF} was often negative, suggesting more variable, or less persistent GPP than PAR$_B$,

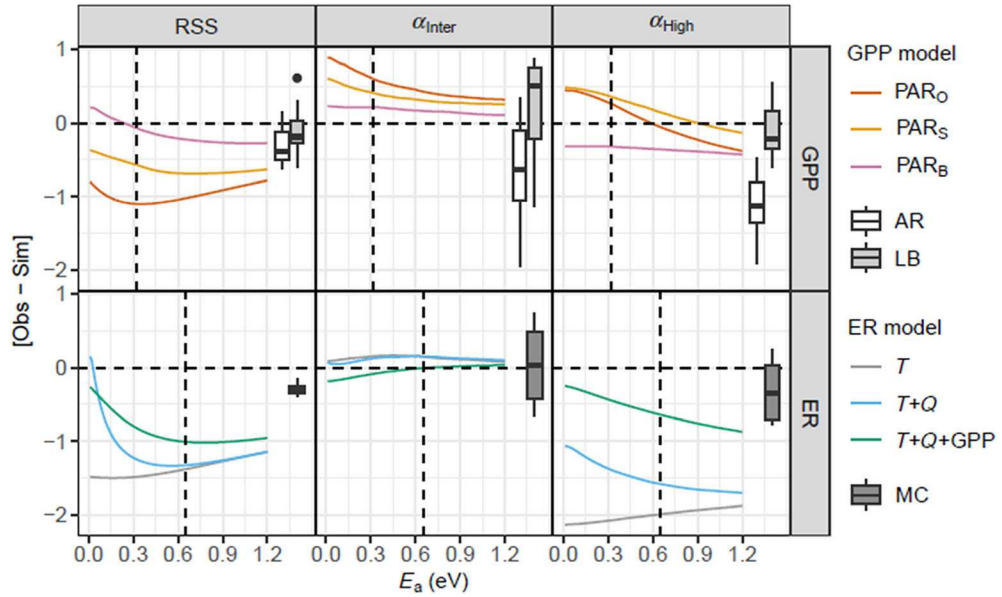

Fig. 5. Frequency-domain model performance for predictions of GPP ($n = 50$; top) and ER ($n = 74$; bottom) with varying temperature sensitivity (E_a) reflected by the cross-site mean difference between observation and simulation ([Obs − Sim]) for relative strength of seasonality (RSS) (left) and spectral slopes at intermediate (α_{Inter}; middle) and high (α_{High}; right) frequency ranges. Inset boxplots are the frequency-domain model performance of autoregressive (AR, gray) and latent biomass (LB, white) GPP models of Blaszczak et al. (2023) ($n = 12$) and the ER model of Bertuzzo et al. (2022) using multiple carbon sources (MC, dark gray; $n = 4$). Horizontal and vertical dashed lines indicate [Obs − Sim] = 0 and theoretical activation energies of ecosystem metabolism ($E_{a,GPP} = 0.32$ eV, $E_{a,ER} = 0.65$ eV), respectively. The GPP model (Eq. 4) informed by PAR_B performed best and was not affected by temperature sensitivity at intra-annual scales. In contrast, RSS and α_{High} for ER were best predicted with the model that included Q and GPP (Eq. 7) when $E_{a,ER} \approx 0$.

implying processes that amplify short-term GPP variability, such as high-flow benthic disturbance (Uehlinger 2006).

Seasonality of PAR_S was greater than GPP (Fig. 2a), overestimating RSS_{GPP} when using PAR_S in Eq. 4 (Fig. 4a, left). At high frequency, PAR_S variance aligned with GPP (Fig. 3) with more sites showing $\alpha_{TF,High} \approx 0$ than PAR_B (Supporting Information Table S4). However, $\alpha_{TF,High}$ was underestimated using PAR_S (Fig. 4a, right), suggesting PAR_S may not control high-frequency GPP variance. Across A_P values (GPP vs. irradiance slope), simulations using PAR_S consistently overestimated RSS and were highly sensitive to A_P, while simulations using PAR_B were insensitive (Supporting Information Fig. S7), supporting weak PAR_S association with GPP variance.

ER spectral properties consistently aligned with GPP across frequencies (Figs. 2, 3), supporting recent modeling showing GPP controls ER variance despite multiple C sources (Bertuzzo et al. 2022). Notably, ER is always more variable than GPP across frequencies (negative α_{TF} between ER and GPP; Fig. 3), converse to presumed temporal stability of ER relative to GPP (O'Donnell and Hotchkiss 2022), implying high-frequency effects on ER variance from external forcings (Roberts et al. 2007; Demars 2019). Regardless of mechanisms, however, ER variation is clearly coupled to productivity regimes.

Temperature was a negligible driver of metabolic variation, with far stronger seasonality than GPP ($RSS_T \gg RSS_{GPP}$) (Fig. 2b), and dramatic divergence in high-frequency persistence ($\alpha_{TF,High} \ll 0$) (Fig. 3) due to thermal inertia (Grbić et al. 2013). Better alignment was observed at intermediate frequency ($\alpha_{TF,Inter} \approx 0$), potentially implying T effects on metabolic variation within certain frequencies but more likely reflecting spectral alignment of T and PAR_B. Limited T impact was reinforced by GPP model insensitivity to $E_{a,GPP}$ when using PAR_B (Fig. 5, top row). Our model results also suggest minimal T control on respiration regimes given elevated ER model performance when neglecting T ($E_{a,ER} \approx 0$) (Fig. 5, bottom row).

Q effects varied with watershed size, with high-frequency alignment between metabolism (both GPP and ER) and Q for smaller watersheds (Supporting Information Fig. S8). This is likely a residence time effect, with increased high-frequency persistence of Q (i.e., steeper α_{High}) in larger watersheds (Hensley et al. 2018). That is, discharge controls on fine-scale metabolic variation are more prominent in smaller rivers, where Q imposes greater variation in light regimes (Savoy and Harvey 2021), benthic scour (Uehlinger 2006), and supply rates of nutrients and OM (Diamond and Cohen 2018).

The drivers of metabolic regimes inferred here align with controls on spatial variation in annual GPP (light) and ER (GPP), including omission of T (Bernhardt et al. 2022). However, temporal correlations between metabolism and drivers were poor (Supporting Information Fig. S4), yielding limited discriminatory information about drivers. For example, all light inputs were equally correlated with GPP, and GPP and T were equally correlated with ER. This highlights the utility

of frequency-domain analysis to examine temporal structures and embedded controls of metabolism by revealing energy inputs (PAR_B and GPP) as important controls on GPP and ER variations.

Improving metabolism models

Frequency-domain analysis yielded novel inferences about metabolism models. For example, the GPP model (Eq. 4) best captured observed variance structures using PAR_B (Fig. 4a), with weaker alignment using PAR_O and PAR_S, prioritizing water-column light attenuation when predicting GPP (Kirk et al. 2021; Savoy and Harvey 2021). Frequency-domain results from Blaszczak et al. (2023) suggest including latent biomass captured observed variance structures better than autoregressive model (Fig. 5, top row), highlighting a significant advance for replicating frequency-domain patterns. Given our PAR_B model also performed well in the frequency domain, using PAR_B in the LB model is likely to further improve performance.

ER model predictions aligned better with observations when including both Q and GPP drivers (Eq. 7), and when neglecting T effects (i.e., low E_a, Fig. 5, bottom row). Comparable frequency-domain alignment of our ER model to Bertuzzo et al. (2022) despite stark differences in time-domain goodness-of-fit (Supporting Information Figs. S5, S6; Table S6) supports continued ER model refinement including time-varying multiple C sources (Bertuzzo et al. 2022) rather than metabolic first principles that neglect supply variation (Song et al. 2018).

Frequency-domain analysis characterizes the metabolic regime of rivers. Our analysis revealed regime attributes relevant to predictions across time scales, including fractal scaling and variance alignment to discriminate among drivers (e.g., PAR_S vs. PAR_B, T vs. C supply). This complements time-domain analyses and provides a novel benchmark for assessing metabolism models.

References

Allen, A. P., J. F. Gillooly, and J. H. Brown. 2005. Linking the global carbon cycle to individual metabolism. Funct. Ecol. **19**: 202–213. doi:10.1111/j.1365-2435.2005.00952.x

Appling, A. P., R. O. Hall, C. B. Yackulic, and M. Arroita. 2018*a*. Overcoming equifinality: Leveraging long time series for stream metabolism estimation. J. Geophys. Res. Biogeosciences **123**: 624–645. doi:10.1002/2017JG004140

Appling, A. P., and others. 2018*b*. The metabolic regimes of 356 rivers in the United States. Sci. Data **5**: 180292. doi:10.1038/sdata.2018.292

Bernhardt, E. S., and others. 2018. The metabolic regimes of flowing waters. Limnol. Oceanogr. **63**: S99–S118. doi:10.1002/lno.10726

Bernhardt, E. S., and others. 2022. Light and flow regimes regulate the metabolism of rivers. Proc. Natl Acad. Sci. USA **119**: e2121976119. doi:10.1073/pnas.2121976119

Bertuzzo, E., E. R. Hotchkiss, A. Argerich, J. S. Kominoski, D. Oviedo-Vargas, P. Savoy, R. Scarlett, D. von Schiller, and J. B. Heffernan. 2022. Respiration regimes in rivers: Partitioning source-specific respiration from metabolism time series. Limnol. Oceanogr. **67**: 2374–2388. doi:10.1002/lno.12207

Blaszczak, J. R., C. B. Yackulic, R. K. Shriver, and R. O. Hall. 2023. Models of underlying autotrophic biomass dynamics fit to daily river ecosystem productivity estimates improve understanding of ecosystem disturbance and resilience. Ecol. Lett. **26**: 1510–1522. doi:10.1111/ele.14269

Brown, J. H., J. F. Gillooly, A. P. Allen, V. M. Savage, and G. B. West. 2004. Toward a metabolic theory of ecology. Ecology **85**: 1771–1789. doi:10.1890/03-9000

Cazelles, B., M. Chavez, G. C. D. Magny, J.-F. Guégan, and S. Hales. 2007. Time-dependent spectral analysis of epidemiological time-series with wavelets. J. R. Soc. Interface **4**: 625–636. doi:10.1098/rsif.2007.0212

Demars, B. O. L. 2019. Hydrological pulses and burning of dissolved organic carbon by stream respiration: Hydrological pulses and stream respiration. Limnol. Oceanogr. **64**: 406–421. doi:10.1002/lno.11048

Diamond, J. S., and M. J. Cohen. 2018. Complex patterns of catchment solute–discharge relationships for coastal plain rivers. Hydrol. Process. **32**: 388–401. doi:10.1002/hyp.11424

Diamond, J. S., F. Moatar, M. J. Cohen, A. Poirel, C. Martinet, A. Maire, and G. Pinay. 2022. Metabolic regime shifts and ecosystem state changes are decoupled in a large river. Limnol. Oceanogr. **67**: S54-S70. doi:10.1002/lno.11789

Dodds, W. K., B. J. FBiggs, and R. L. Lowe. 1999. Photosynthesis-irradiance patterns in benthic microalgae: Variations as a function of assemblage thickness and community structure. J. Physiol. **35**: 42–53. doi:10.1046/j.1529-8817.1999.3510042.x

Fasching, C., A. J. Ulseth, J. Schelker, G. Steniczka, and T. J. Battin. 2016. Hydrology controls dissolved organic matter export and composition in an Alpine stream and its hyporheic zone. Limnol. Oceanogr. **61**: 558–571. doi:10.1002/lno.10232

Grbić, R., D. Kurtagić, and D. Slišković. 2013. Stream water temperature prediction based on Gaussian process regression. Expert Syst. Appl. **40**: 7407–7414. doi:10.1016/j.eswa.2013.06.077

Halley, J. M. 1996. Ecology, evolution and 1/f-noise. Trends Ecol. Evol. **11**: 33–37. doi:10.1016/0169-5347(96)81067-6

Hensley, R. T., M. J. Cohen, and J. W. Jawitz. 2018. Channel filtering generates multifractal solute signals. Geophys. Res. Lett. **45**: 11722–11731. doi:10.1029/2018GL079864

Jassby, A. D., and T. Platt. 1976. Mathematical formulation of the relationship between photosynthesis and light for phytoplankton: Photosynthesis-light equation. Limnol. Oceanogr. **21**: 540–547. doi:10.4319/lo.1976.21.4.0540

Julian, J. P., S. Z. Seegert, S. M. Powers, E. H. Stanley, and M. W. Doyle. 2011. Light as a first-order control on ecosystem structure in a temperate stream. Ecohydrology **4**: 422–432. doi:10.1002/eco.144

Kirchner, J. W., and C. Neal. 2013. Universal fractal scaling in stream chemistry and its implications for solute transport and water quality trend detection. Proc. Natl Acad. Sci. USA **110**: 12213–12218. doi:10.1073/pnas.1304328110

Kirk, L., R. T. Hensley, P. Savoy, J. B. Heffernan, and M. J. Cohen. 2021. Estimating benthic light regimes improves predictions of primary production and constrains light-use efficiency in streams and rivers. Ecosystems **24**: 825–839. doi:10.1007/s10021-020-00552-1

Koenig, L. E., A. M. Helton, P. Savoy, E. Bertuzzo, J. B. Heffernan, R. O. Hall, and E. S. Bernhardt. 2019. Emergent productivity regimes of river networks. Limnol. Oceanogr. Lett. **4**: 173–181. doi:10.1002/lol2.10115

Molénat, J., P. Davy, C. Gascuel-Odoux, and P. Durand. 1999. Study of three subsurface hydrologic systems based on spectral and cross-spectral analysis of time series. J. Hydrol. **222**: 152–164. doi:10.1016/S0022-1694(99)00107-9

O'Donnell, B., and E. R. Hotchkiss. 2022. Resistance and resilience of stream metabolism to high flow disturbances. Biogeosciences **19**: 1111–1134. doi:10.5194/bg-19-1111-2022

Odum, H. T. 1956. Primary production in flowing Waters1. Limnol. Oceanogr. **1**: 102–117. doi:10.4319/lo.1956.1.2.0102

Parkhill, K. L., and J. S. Gulliver. 1999. Modeling the effect of light on whole-stream respiration. Ecol. Model. **117**: 333–342. doi:10.1016/S0304-3800(99)00017-4

R Core Team. 2013. R: A language and environment for statistical computing. R Foundation for Statistical Computing.

Roberts, B. J., P. J. Mulholland, and W. R. Hill. 2007. Multiple scales of temporal variability in ecosystem metabolism rates: Results from 2 years of continuous monitoring in a forested headwater stream. Ecosystems **10**: 588–606. doi:10.1007/s10021-007-9059-2

Savoy, P., A. P. Appling, J. B. Heffernan, E. G. Stets, J. S. Read, J. W. Harvey, and E. S. Bernhardt. 2019. Metabolic rhythms in flowing waters: An approach for classifying river productivity regimes. Limnol. Oceanogr. **64**: 1835–1851. doi:10.1002/lno.11154

Savoy, P., and J. W. Harvey. 2021. Predicting light regime controls on primary productivity across CONUS river networks. Geophys. Res. Lett. **48**: e2020GL092149. doi:10.1029/2020GL092149

Segatto, P. L., T. J. Battin, and E. Bertuzzo. 2020. Modeling the coupled dynamics of stream metabolism and microbial biomass. Limnol. Oceanogr. **65**: 1573–1593. doi:10.1002/lno.11407

Shin, Y. 2024. Collected data for Shin and others (2024): Energy inputs imprint seasonality and fractal scaling on river metabolic regimes [Dataset]. HydroShare. doi:10.4211/hs.6663122ba06749ac92409ff53f81af7c

Song, C., and others. 2018. Continental-scale decrease in net primary productivity in streams due to climate warming. Nat. Geosci. **11**: 415–420. doi:10.1038/s41561-018-0125-5

Stoica, P., and R. L. Moses. 2005. *Spectral analysis of signals*, v. **452**. Pearson Prentice Hall.

Stoy, P. C., and others. 2009. Biosphere-atmosphere exchange of CO_2 in relation to climate: A cross-biome analysis across multiple time scales. Biogeosciences **6**: 2297–2312. doi:10.5194/bg-6-2297-2009

Thompson, S. E., and G. G. Katul. 2012. Multiple mechanisms generate Lorentzian and 1/fα power spectra in daily streamflow time series. Adv. Water Resour. **37**: 94–103. doi:10.1016/j.advwatres.2011.10.010

Uehlinger, U. 2006. Annual cycle and inter-annual variability of gross primary production and ecosystem respiration in a floodprone river during a 15-year period. Freshw. Biol. **51**: 938–950. doi:10.1111/j.1365-2427.2006.01551.x

Vannote, R. L., G. W. Minshall, K. W. Cummins, J. R. Sedell, and C. E. Cushing. 1980. The river continuum concept. Can. J. Fish. Aquat. Sci. **37**: 130–137. doi:10.1139/f80-017

Vasseur, D. A., and P. Yodzis. 2004. The color of environmental noise. Ecology **85**: 1146–1152. doi:10.1890/02-3122

Acknowledgments

We thank the US Geological Survey, the authors of Appling et al. (2018*b*), Blaszczak et al. (2023), Bertuzzo et al. (2022), and Harvey and Savoy (2022) for making datasets publicly available. Funding support was from the University of Florida Water Institute Graduate Fellowship and the National Science Foundation Award #2000649.

Submitted 13 October 2023
Revised 21 May 2024
Accepted 01 June 2024